NeuroImage: Clinical 19 (2018) 805–812

Contents lists available at ScienceDirect

NeuroImage: Clinical

journal homepage: www.elsevier.com/locate/ynicl

Isolated focal dystonia phenotypes are associated with distinct patterns of altered microstructure

Brian D. Berman[a,b,c,*], Justin M. Honce[b], Erica Shelton[b], Stefan H. Sillau[b], Lidia M. Nagae[b,d]

[a] Department of Neurology, University of Colorado School of Medicine, Aurora, CO, United States
[b] Department of Radiology, University of Colorado School of Medicine, Aurora, CO, United States
[c] Neurology Section, Denver VA Medical Center, Denver, CO, United States
[d] Department of Radiology, University of Florida, Gainesville, FL, United States

ARTICLE INFO

Keywords:
Blepharospasm
Cervical dystonia
Diffusion tensor imaging
Basal ganglia
Cerebellum

ABSTRACT

Objective: Isolated adult-onset focal dystonia is considered a network disorder with disturbances to the motor basal ganglia and cerebellar circuits playing a pathophysiological role, but why specific body regions become affected remains unknown. We aimed to use diffusion tensor imaging to determine if the two most common phenotypes of focal dystonia are associated with distinguishing microstructural changes affecting the motor network.

Methods: Fifteen blepharospasm patients, 20 cervical dystonia patients, and 30 age- and sex-matched healthy controls were recruited. Maps of fractional anisotropy and mean diffusivity were analyzed using a voxel-based approach and an automated region-of-interest technique to evaluate deep gray matter nuclei. Correlations between diffusion measures and dystonia severity were tested, and post hoc discriminant analyses were conducted.

Results: Voxel-based analyses revealed significantly reduced fractional anisotropy in the right cerebellum and increased mean diffusivity in the left caudate of cervical dystonia patients compared to controls, as well as lower fractional anisotropy in the right cerebellum in cervical dystonia patients relative to blepharospasm patients. In addition to reduced fractional anisotropy in the bilateral caudate nucleus of cervical dystonia patients relative to controls and blepharospasm patients, region-of-interest analyses revealed significantly reduced fractional anisotropy in the right globus pallidus internus and left red nucleus of blepharospasm patients compared to both controls and cervical dystonia patients. Diffusivity measures in the red nucleus of blepharospasm patients correlated with disease severity. In a three-group discriminant analysis, participants were correctly classified with only modest reliability (67–75%), but in a two-group discriminant analysis, patients could be distinguished from each other with high reliability (83–100%).

Conclusions: Different focal dystonia phenotypes are associated with distinct patterns of altered microstructure within constituent regions of basal ganglia and cerebellar circuits.

1. Introduction

Isolated adult-onset focal dystonias are a heterogeneous group of diseases that may share overlapping etiologies, yet present with distinct clinical features (Jinnah et al., 2013). Blepharospasm (BSP) and cervical dystonia (CD), defined by dystonia affecting eyelid and neck muscles respectively, are the two most common forms of adult-onset focal dystonia. The precise etiology and pathophysiology of BSP and CD remain incompletely understood. Several gene mutations have been identified (Lohmann and Klein, 2017), but these account for only a very small percentage of those affected. And while pathological abnormalities involving the basal ganglia, brainstem and cerebellum have frequently been linked to secondary forms of dystonia including BSP and CD (Jinnah et al., 2017), relatively few cases of isolated BSP and CD have been studied pathologically with most reporting little or no detectable neuropathology (Jinnah et al., 2017; Standaert, 2011). In contrast, neuroimaging studies in isolated forms of focal dystonia have provided in vivo evidence of microstructural abnormalities within and between these brain regions supporting that motor network dysfunction likely plays a role in their pathophysiology (Lehéricy et al., 2013; Neychev et al., 2011; Zoons et al., 2011). To date, findings from microstructural imaging studies in isolated adult-onset focal dystonia,

Abbreviations: BSP, blepharospasm; CD, cervical dystonia; DTI, diffusion tensor imaging; FA, fractional anisotropy; HC, healthy control; JRS, Jankovic Rating Scale; MD, mean diffusivity; MNI, Montreal Neurological Institute; ROI, region of interest; TWSTRS, Toronto Western Spasmodic Torticollis Rating Scale

* Corresponding author at: University of Colorado Anschutz Medical Campus, Department of Neurology, 12631 E. 17th Avenue, Mail Stop B-185, Aurora, CO 80045, United States.
E-mail address: brian.berman@ucdenver.edu (B.D. Berman).

https://doi.org/10.1016/j.nicl.2018.06.004
Received 2 March 2018; Received in revised form 17 May 2018; Accepted 3 June 2018
Available online 05 June 2018

however, have identified diverse and at times inconsistent findings, possibly stemming from the inclusion of multiple dystonia phenotypes or differences in the tissue types or brain regions being investigated. Better characterization of the microstructural changes associated with different focal dystonia phenotypes could improve our understanding of the neurobiological mechanisms underlying dystonia and help elucidate whether different phenotypes are associated with distinct pathological motor networks disruptions.

Diffusion tensor imaging (DTI) is a MR-based imaging technique that enables in vivo mapping of the diffusion of water molecule in biological tissues. While DTI measures are frequently used to reveal integrity of white matter tracts, DTI can also be used to investigate the microstructural integrity of deep gray matter brain structures and provide insight into the cellular density and arrangement within nuclei (Vaillancourt et al., 2009). DTI measures most often include fractional anisotropy (FA), which provides an estimate of the degree of directionality of water diffusion and reflects the coherence of nerve fibers, and mean diffusivity (MD), which is a measure largely influenced by cell density and distribution of the extracellular space.

Although DTI studies to date have revealed variable and at times conflicting results in isolated focal dystonia, microstructural brain abnormalities have been most frequently reported in the basal ganglia, cerebellum, and sensorimotor cortex (Lehéricy et al., 2013; Neychev et al., 2011; Ramdhani and Simonyan, 2013; Zoons et al., 2011). In one early DTI study of CD, Colosimo et al. reported increased FA in the putamina of CD patients compared to healthy controls (HC) (Colosimo et al., 2005). This finding was duplicated by Fabbrini et al. in a larger cohort of CD patients and HC, with additional reporting of decreased MD in other basal ganglia (Fabbrini et al., 2008). Interestingly, Fabbrini et al. found no significant DTI changes in a BSP group compared to HC suggesting that microstructural differences may exist between different adult-onset focal dystonia phenotypes. More recently, Pinheiro et al. reported finding no differences in DTI measures between HC and patients with either BSP or CD (Pinheiro et al., 2015), however their study focused on evaluating white matter changes and was limited by small numbers of patients in the BSP group.

Although voxel-based analyses of DTI data can be used to investigate microstructural changes across the brain within the white matter as well as the gray matter, they require spatial normalization procedures and correction for multiple comparisons that can limit its ability to detect changes within smaller deep gray matter structures like the globus pallidus and substantia nigra. Region of interest (ROI) analyses of DTI data, however, require highly accurate placement of the ROIs to avoid inclusion of white matter and erroneous results. Combining these two analysis approaches can often lead to a more comprehensive understanding of the pathophysiology underlying neurologic and psychiatric disorders (Schwarz et al., 2013; Snook et al., 2007; Srivastava et al., 2016; Wang et al., 2008).

Our aim in this study was to analyze DTI data collected on BSP patients, CD patients and HC using a whole-brain voxel-based analysis and an automated and verified ROI placement approach based on high-resolution probabilistic atlas maps to determine whether there are microstructural changes are present within cortical regions of the brain and deep gray matter nuclei in patients with BSP and CD. Additionally, we aimed to test whether microstructural differences exist between BSP and CD and whether they correlate with severity of the dystonia phenotype. Based on the findings from prior analogous studies, we hypothesized that BSP and CD would be associated with a distinct DTI pattern of microstructural changes, and that some of these changes could be linked to dystonia severity.

2. Materials and methods

2.1. Participants

Thirty-five patients with isolated, adult-onset focal dystonia (15 BSP and 20 CD) and 30 HC were recruited for this study. Dystonia patients were recruited from the University of Colorado Movement Disorders Center, and age- and sex-matched HC were recruited from patient spouses and the local community. Participants were excluded if they were taking any medication associated with causing dystonia, had any contraindications to MRI, or had cognitive impairment as evidenced by a Montreal Cognitive Assessment score < 26 (Damian et al., 2011). Patients were excluded if they had a history of dystonia beginning prior to age 18, as childhood onset dystonia typically represents a more generalized form of dystonia, or exposure to anti-dopaminergic medications, had undergone deep brain stimulation surgery, or had severe dystonia to limit confounding of imaging data and motion effects. Patients receiving treatment with botulinum toxin injections were scanned no sooner than 10 weeks following their last injections. Dystonia severity was assessed on the day of scanning using phenotype-specific scales of the Jankovic Rating Scale (JRS) for BSP (Jankovic et al., 2009), and the Toronto Western Spasmodic Torticollis Rating Scale (TWSTRS) for CD (Consky and Lang, 1994).

All participants underwent a neurological examination. HC were excluded if they had any abnormal neurological findings. In order to include as pure of dystonia phenotypes as possible, patients were removed from the study if they had any evidence of dystonia affecting a body region beyond their primary diagnosis. This led to the removal of three BSP patients and two CD patients from subsequent analyses. In total, 12 patients with BSP, 18 patients with CD, and 30 HC were included in the final analysis (Table 1). All participants gave written informed consent for the research protocol, which was approved by the Colorado Multiple Institutional Review Board.

2.2. DTI acquisition

Eight BSP patients, 10 CD patients, and 15 HC were scanned on a GE Signa HDxt 3 T MRI scanner (GE Medical Systems, Milwaukee, WI) with an 8-channel brain phased-array head coil, using a 32-direction spin

Table 1
Participant demographics of those included in final DTI analysis.

	Participants			Group comparisons (p Values)		
	HC ($n = 30$)	BSP ($n = 12$)	CD ($n = 18$)	BSP vs HC	CD vs HC	BSP vs CD
Age, y	62.6 ± 7.0	62.7 ± 8.4	62.6 ± 8.2	0.981	0.996	0.986
Sex, F	21 (70%)	14 (78%)	8 (67%)	1.000	0.740	0.678
Scanner, GE	17 (67%)	8 (67%)	10 (56%)	0.731	0.940	0.709
Disease duration, y	–	8.1 ± 7.3	17.6 ± 15.3	–	–	0.032
JRS	–	10.7 ± 4.8	–	–	–	–
TWSTRS	–	–	21.3 ± 8.4	–	–	–

Values shown as mean ± sd, except for sex and scanner where the frequency and percentage are presented. p values calculated using two-tailed independent sample t-tests with Satterthwaite method for unequal variances, except for sex and scanner differences tested using chi-square test or Fisher's exact test. Abbreviations: BSP = blepharospasm; CD = cervical dystonia; HC = healthy control; JRS = Jankovic Rating Scale; TWSTRS = Toronto Western Spasmodic Torticollis Scale.

echo, and echo planar imaging DTI sequence with TR/TE = 16,000/92 ms. The remaining 4 BSP patients, 8 CD patients, and 15 HC were scanned on a replacement Siemens Skyra 3 T MRI scanner with a 20-channel phased-array RF neurovascular coil, using a 30-direction spin echo, and echo planar imaging DTI sequence with TR/TE = 8500/75 ms. All scans were acquired with a 128 × 128 matrix size, slice thickness = 2 mm, and included images with b values of 0 and 1000 s/mm^2.

2.3. Image analysis

All image analysis was performed using the Functional Magnetic Resonance Imaging of the Brain (FMRIB; www.fmrib.ox.ac.uk/fsl) Software Library tools (FSL) and SPM8 (www.fil.ion.ucl.ac.uk/spm). The b0 image was used for estimation of the inhomogeneity fields and motion and eddy current-induced geometric distortions were removed with the *eddy_correct* tool in FMRIB's Diffusion Toolbox. Using the DTIfit tool, the eddy current corrected DTI data for each subject was processed to generate voxel-wise maps of FA and MD. No masking or thresholding to define white and gray matter was performed. The individual subject maps were then normalized to 1mm^3 Montreal Neurological Institute (MNI) 152 standard space using Linear Registration Tools followed by Non-linear Image Registration Tools. Voxel-based analyses were performed in SPM8 using normalized FA and MD maps resampled to 2mm^3 and smoothed using an isotropic Gaussian filter (8-mm full width at half maximum).

Microstructural alterations within deep gray matter nuclei were investigated using an automated ROI placement approach to limit the variability in ROI placement which can occur with manual approaches. All ROI masks were initially extracted from an ultra-high resolution probabilistic map acquired on a 7 T MRI scanner (Keuken et al., 2014). First, the probabilistic atlas was down-sampled from 0.4 × 0.4 × 0.4 mm^3 to 1 mm^3 in MNI 152 space using the FLIRT tool. Using FSLView, probabilistic ROI masks were extracted from labels for the bilateral caudate, putamen, globus pallidus externus, globus pallidus internus, subtantia nigra, red nucleus, and subthalamic nucleus. The extracted probabilistic ROI masks were then thresholded using the *fslmaths* tool to a probability of 80% to avoid overlap with adjacent anatomical structures.

Following the creation of standard space ROI masks for each subcortical structure as detailed above, the ROI masks were individually transposed into the native subject space for each study participant. First the FMIRB's *invwarp* tool was used to calculate the inverse warps of the previously performed non-linear registration of each study participants' FA maps to MNI standard space. The *applywarp* tool was then applied to the resulting inverse warps to convert all thresholded, standard space masks to native subject space for each study participant. A blinded quality assessment review was then performed by a board-certified neuroradiologist (L.M.N.) in which the ROIs in subject space were superimposed on each subject's FA map to confirm the final accuracy of the ROI placement. Following the blinded qualitative assessment, the FMRIB's *fslstats* tool was used to apply the participant-specific subject space masks for each subcortical structure to their voxel-wise maps of FA and MD and extract the mean values.

2.4. Statistical analyses

Demographic variables were compared using two-tailed *t*-tests, F tests, and chi-squared tests as appropriate using the Satterthwaite method for unequal variances. Significance was set to $p < 0.05$ for these comparisons. Our primary imaging aim was to investigate microstructural differences between BSP and CD patients when compared to HC. Voxel-wise differences in FA and MD among the three groups were analyzed using regression models and two-sample *t*-tests in SPM8 to identify differences of FA and MD in BSP vs. HC, CD vs. HC, and BSP vs. CD. Scanner type was included as a covariate and significance threshold at the voxel level was set at $p < 0.001$, followed by cluster-level threshold $\alpha < 0.05$, corrected for multiple comparisons using *3dClustSim* as implemented in AFNI (https://afni.nimh.nih.gov) version 16.3.15.

Differences in FA and MD within deep gray matter nuclei ROIs among the three groups were analyzed using regression models for each structure, with group controlled for age, sex, and scanner type. Residual variance was allowed to vary by group and Satterthwaite degrees of freedom were used. To reduce the overall number of comparisons made, an overall F test for adjusted mean differences among the groups was performed for each structure and DTI measure, and if the F test was significant it was followed by post hoc t-tests to identify differences of FA and MD in BSP vs. HC, CD vs. HC, and BSP vs. CD with a Tukey-Kramer adjustment to control the family-wise error rate for all pair-wise comparisons among groups. Statistical analyses were performed except as when stated above using SAS 9.4.

2.5. Correlation analyses

We performed a voxel-based linear regression analysis with the patient DTI maps using JRS scores for BSP patients and TWSTRS scores for CD patients as regressors to identify regions across the brain where microstructural changes correlated with disease duration and dystonia severity. Scanner type was included as a covariate and the significance threshold was set to $p < 0.005$ at the voxel level and corrected for multiple comparisons using *3dClustSim* to cluster-level threshold of $\alpha < 0.05$. To test whether FA and MD values within deep gray matter structures correlated with clinical measures, we performed partial Pearson correlations by group (BSP and CD) adjusted for age, gender, and MRI scanner. Significance threshold for the partial correlations was set to $p < 0.05$. To limit the overall number of correlations investigated, we tested for correlations only for those gray matter structures showing significant group differences in the adjusted regression analysis. Violations of linearity and outliers were checked using scatter plots, histograms, and QQplots.

2.6. Discriminant analyses

In an exploratory post hoc analysis, we aimed to test the ability of our ROI-based DTI results to discriminate between groups. DTI data from ROIs were chosen for the discriminant analysis as they are extracted from an individual subject in their native space and therefore more representative of an individual subject and with greater potential to become a generalizable imaging marker. Candidate discriminant variables were selected by considering whether mean differences existed between the groups in the adjusted regression analysis. Regression was used to remove the effects of age, sex, and scanner on the DTI measurements, and discriminant analyses were applied to the residuals. Parametric (Gaussian based) discriminant analysis was considered so we could create relatively simple and geometrically interpretable discriminant functions, and because the small sample sizes limited the utility of kernel density estimation. Separate covariance matrices by group were allowed, resulting in quadratic (parabolic) discriminant functions. Discriminant functions were evaluated for predictive accuracy using re-substitution and leave-one-out cross validation methods, which can create accurate classifiers even with smaller sample sizes (Zollanvaria et al., 2009). Re-substitution uses all the available data, but can suffer from over-fitting and while it may perform well on available data it may perform poorly on a future unseen test dataset. Leave-one-out cross validation is often applied when there are limited available data and can give a less biased estimate of accuracy, but high variance can lead to unreliable estimates.

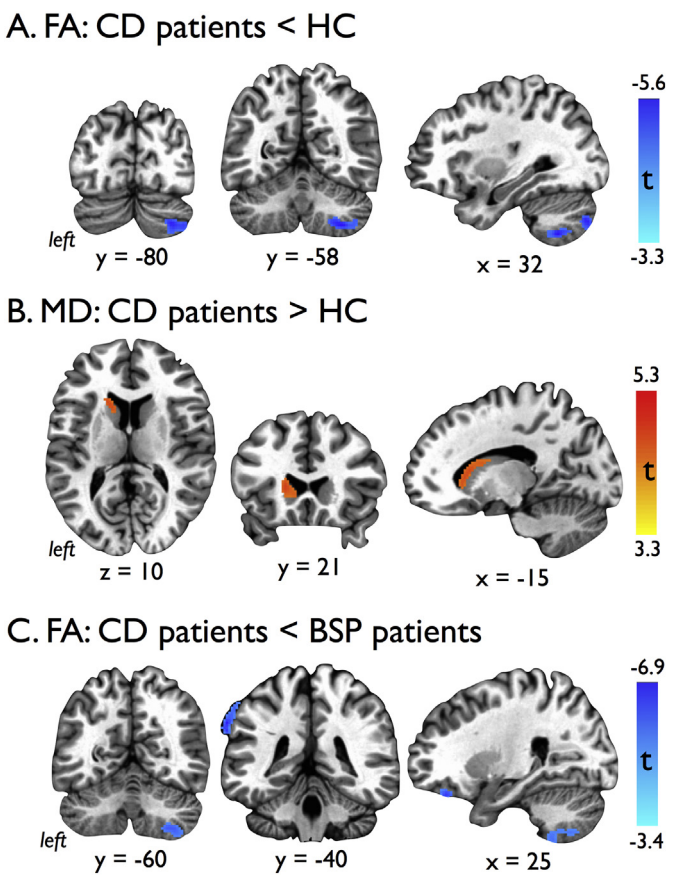

Fig. 1. Results of voxel-based analyses showing A) cluster of reduced fractional anisotropy (FA) within the right cerebellum of cervical dystonia (CD) patients compared to healthy controls (HC), B) cluster of increased mean diffusivity (MD) within the left caudate nucleus in CD patients compared to HC, and C) clusters of decreased FA in the right cerebellum, left supramarginal gyrus, and right inferior frontal gyrus of CD patients compared to blepharospasm (BSP) patients. Voxel-based findings cluster thresholded for an overall $p < 0.05$, FWE corrected.

3. Results

3.1. Participant characteristics

Participant demographics are shown in Table 1. There were no significant differences in age or gender across the three groups of participants. There was no significant difference in overall dystonia severity, but CD patients did have a statistically significant longer disease duration than BSP patients ($p = 0.032$).

3.2. Voxel-based DTI comparisons

In our voxel-based analyses, we identified significant clusters of reduced FA in the right cerebellar cortex (Fig. 1A, Table 2) and increased MD in the left caudate (Fig. 1B, Table 2) in CD patients compared to HC. No significant differences were seen in the contrasts of FA and MD between BSP patients and HC. In the contrast between BSP and CD patients, lower FA in the right cerebellar cortex, left supramarginal gyrus, and right inferior frontal gyrus was seen in the CD patients (Fig. 1C, Table 2). Additionally, no significant differences were seen across subject type ($p = 0.805$), age ($p = 0.367$) or sex ($p = 0.226$) between subjects scanned on the GE Sigma versus those scanned on the Siemens Skrya.

Table 2
Anatomical localization of significant clusters identified in voxel-based DTI analysis.

Contrast	Brain region	MNI Coordinates			Cluster size (voxels)	Peak t value
		X	Y	Z		
FA: CD < HC	Rt Cerebellum (lobules VIII/VII, Crus 2)	32	−58	−54	562	−4.80
MD: CD > HC	Lt Caudate nucleus	−18	22	6	170	4.34
FA: CD < BSP	Rt Cerebellum (lobules VIII/VII, Crus 2)	30	−58	−54	511	−4.76
	Lt Supramarginal gyrus	−68	−38	36	260	−5.94
	Rt Inferior frontal gyrus	24	36	−24	135	−5.21

Results from voxel-based comparisons corrected for multiple comparisons at the cluster level using individual voxel threshold $p < 0.001$ and cluster size $k = 92$. Abbreviations: BSP = blepharospasm; CD = cervical dystonia; FA = fractional anisotropy; HC = healthy control; Lt = left; MD = mean diffusivity; Rt = right.

3.3. ROI-based DTI comparisons

Table 3 shows the results of regression adjusted testing of DTI measures within subcortical gray matter structures across groups of HC and patients with BSP and CD followed by pairwise group testing results. Significant group differences in FA were seen in the bilateral caudate, right globus pallidus internus, right subthalamic nucleus, and left red nucleus, while significant group differences in MD were seen in the left caudate and left red nucleus. Pairwise comparisons showed that group differences were driven by lower FA and higher MD in the caudate of CD patients, and by lower FA in the globus pallidus internus and red nucleus of BSP patients. Group differences in the subthalamic nucleus were driven by higher FA in BSP patients.

3.4. Correlations

There were no significant clusters found in our voxel-based correlation analyses with JRS in BSP patients and TWSTRS in CD patients. In our ROI-based correlation analyses, a significant negative correlation between FA in the left red nucleus and JRS scores in BSP patients was found (rho = −0.702, $p = 0.035$), along with a corresponding significant positive correlation between MD in the left red nucleus and JRS scores (rho = 0.674, $p = 0.047$). No significant correlations were found between either FA or MD in the caudate and TWSTRS scores in CD patients.

3.5. Discriminant analyses

Using FA within the left red nucleus, the left caudate nucleus, and the right subthalamic nucleus, we performed a post hoc discriminant analysis to determine the ability of these three measures together to distinguish between BSP and CD patients and HC. Using re-substitution, nine of 12 BSP patients (75%), 12 of 18 CD patients (67%), and 22 of 30 HCs (73%) were correctly classified (represented graphically as data distribution clouds in Fig. 2A). Of the misclassified patients, all three BSP patients and five of the six CD patients were classified as HC. The eight misclassified HCs were evenly distributed between BSP and CD. Using leave-one-out cross validation, there was some decrease in predictive accuracy with correct classifications seen in eight of 12 (67%) BSP patients, 10 out of 18 (56%) CD patients, and 19 out of 30 (63%) HCs (Fig. 2B). Three of the four misclassified BSP patients and six of the eight misclassified CD patients were classified as HC. Non-parametric methods for estimating distribution densities with kernels were

Table 3
DTI measures across study subjects.

		Participants			Group comparisons (*p* values)			
		HC	BSP	CD	Overall*	BSP vs HC+	CD vs HC+	BSP vs CD+
FA values								
Caudate	L	0.20 ± 0.03	0.20 ± 0.03	0.18 ± 0.04	0.031	0.995	0.046	0.038
	R	0.21 ± 0.03	0.21 ± 0.03	0.19 ± 0.04	0.027	0.998	0.035	0.044
Putamen	L	0.22 ± 0.05	0.22 ± 0.04	0.22 ± 0.06	0.919	–	–	–
	R	0.21 ± 0.05	0.21 ± 0.04	0.20 ± 0.05	0.294	–	–	–
GPe	L	0.37 ± 0.05	0.37 ± 0.06	0.35 ± 0.07	0.336	–	–	–
	R	0.35 ± 0.07	0.33 ± 0.07	0.33 ± 0.08	0.188	–	–	–
GPi	L	0.57 ± 0.06	0.57 ± 0.06	0.60 ± 0.05	0.193	–	–	–
	R	0.45 ± 0.07	0.42 ± 0.03	0.46 ± 0.06	0.010	0.047	0.821	0.026
STN	L	0.47 ± 0.06	0.53 ± 0.09	0.48 ± 0.08	0.287	–	–	–
	R	0.49 ± 0.05	0.54 ± 0.05	0.50 ± 0.07	0.040	0.039	0.675	0.336
SN	L	0.55 ± 0.09	0.54 ± 0.11	0.52 ± 0.09	0.543	–	–	–
	R	0.53 ± 0.06	0.48 ± 0.08	0.55 ± 0.10	0.185	–	–	–
RN	L	0.53 ± 0.09	0.43 ± 0.9	0.56 ± 0.11	0.004	0.013	0.710	0.008
	R	0.49 ± 0.08	0.51 ± 0.13	0.52 ± 0.09	0.344	–	–	–
MD values								
Caudate	L	1.14 ± 0.28	1.07 ± 0.32	1.36 ± 0.47	0.031	0.509	0.089	0.024
	R	1.03 ± 0.24	1.04 ± 0.23	0.18 ± 0.34	0.138	–	–	–
Putamen	L	0.73 ± 0.06	0.73 ± 0.04	0.76 ± 0.09	0.298	–	–	–
	R	0.72 ± 0.07	0.74 ± 0.07	0.77 ± 0.11	0.132	–	–	–
GPe	L	0.73 ± 0.12	0.77 ± 0.09	0.75 ± 0.11	0.551	–	–	–
	R	0.75 ± 0.13	0.77 ± 0.10	0.78 ± 0.13	0.466	–	–	–
GPi	L	0.57 ± 0.10	0.57 ± 0.09	0.56 ± 0.13	0.956	–	–	–
	R	0.64 ± 0.16	0.64 ± 0.11	0.59 ± 0.16	0.322	–	–	–
STN	L	0.65 ± 0.07	0.64 ± 0.14	0.66 ± 0.12	0.980	–	–	–
	R	0.64 ± 0.08	0.69 ± 0.11	0.65 ± 0.14	0.378	–	–	–
SN	L	0.64 ± 0.12	0.59 ± 0.14	0.68 ± 0.15	0.282	–	–	–
	R	0.68 ± 0.13	0.63 ± 0.11	0.65 ± 0.17	0.246	–	–	–
RN	L	0.59 ± 0.11	0.66 ± 0.09	0.57 ± 0.13	0.035	0.067	0.909	0.091
	R	0.63 ± 0.10	0.67 ± 0.14	0.60 ± 0.13	0.375	–	–	–

Values shown as mean ± sd except where indicated. *p values calculated using protective overall F-test to identify any differences among the three groups. +p values from pairwise comparisons among the groups when F-test was significant (< 0.05) using a Tukey-Kramer adjustment for multiple comparisons. Abbreviations: BSP = blepharospasm; CD = cervical dystonia; FA = fractional anisotropy; GPe/i = globus pallidus externus/internus; HC = healthy control; MD = mean diffusivity; RN = red nucleus; SN = substantia nigra; STN = subthalamic nucleus.

explored, but they performed no better or worse than the classical parametric method.

Using FA measures from the left caudate nucleus and left red nucleus, we conducted a separate exploratory discriminant analysis to assess the ability of these measures to differentiate between BSP and CD patients. These structures were selected because significant differences in FA within them were found between the dystonia subtypes in our adjusted regression analysis, because the data distributions from each separated CD and BSP from HC, respectively, and because their FA values were least correlated. Re-substitution correctly classified all (100%) of the BSP patients and 15 of the 18 (83%) CD patients (Fig. 2C). The region for classifying a patient as BSP was a parabola narrow along the left caudate axis and long along the left red nucleus axis. Results for leave-one-out cross validation were identical to re-substitution except that one of the 12 BSP patients was misclassified (Fig. 2D).

4. Discussion

In this study, we found differing patterns of microstructural abnormalities involving the basal ganglia, brainstem nuclei and cerebellum in the two most common forms of adult-onset isolated focal dystonia. Our voxel-based analysis revealed reduced FA in the right cerebellum and increased MD in the left caudate nucleus of CD patients compared to controls, but no differences in FA or MD between BSP patients and controls. Using a probabilistic atlas-derived ROI-based analysis to investigate microstructural changes within deep gray matter nuclei, however, decreased FA in the left red nucleus and right globus pallidus internus and increased FA in the subthalamic nucleus were found in BSP patients compared to controls. In BSP patients, diffusivity measures within the left red nucleus significantly correlated with dystonia severity. These findings reinforce that microstructural disruptions within nodes of the basal ganglia and cerebellar networks contribute to the pathophysiology of adult-onset focal dystonia and provide evidence that different dystonia phenotypes are associated with distinct and non-overlapping patterns of altered microstructure.

Although no significant voxel-based changes were found that distinguish BSP patients from those with CD and HC, our ROI-based analysis revealed that BSP is associated with reduced FA in the left red nucleus and right globus pallidus internus, and that the changes in the red nucleus were tightly correlated with disease severity. A link between BSP and the red nucleus, where output from the cerebellum and basal ganglia are believed to interact and influence movement of facial muscles (Pong et al., 2008), is supported by in vitro studies and animal investigations. For instance, retrograde transneuronal tracing of a rabies virus injected in the orbicularis oculi muscle of rats demonstrated that a specific pool of neurons in the red nucleus is involved in the motor network of spontaneous, reflex, and learned blinking (Morcuende et al., 2002). Stimulation of the red nucleus in animal models has also been shown to cause eye blink responses and has been explored as an animal model for BSP (Chapman et al., 1988; Klemm et al., 1993; Nowak et al., 1997). As the red nucleus is a key component of the response output circuitry of the cerebellum, our findings add to the growing body of literature supporting a key pathophysiological role of the cerebellum and cerebello-thalamo-cortical networks in dystonia (Bologna and Berardelli, 2017; Kaji et al., 2018; Prudente et al., 2014; Shakkottai et al., 2017).

The validity of our finding microstructural changes within the right

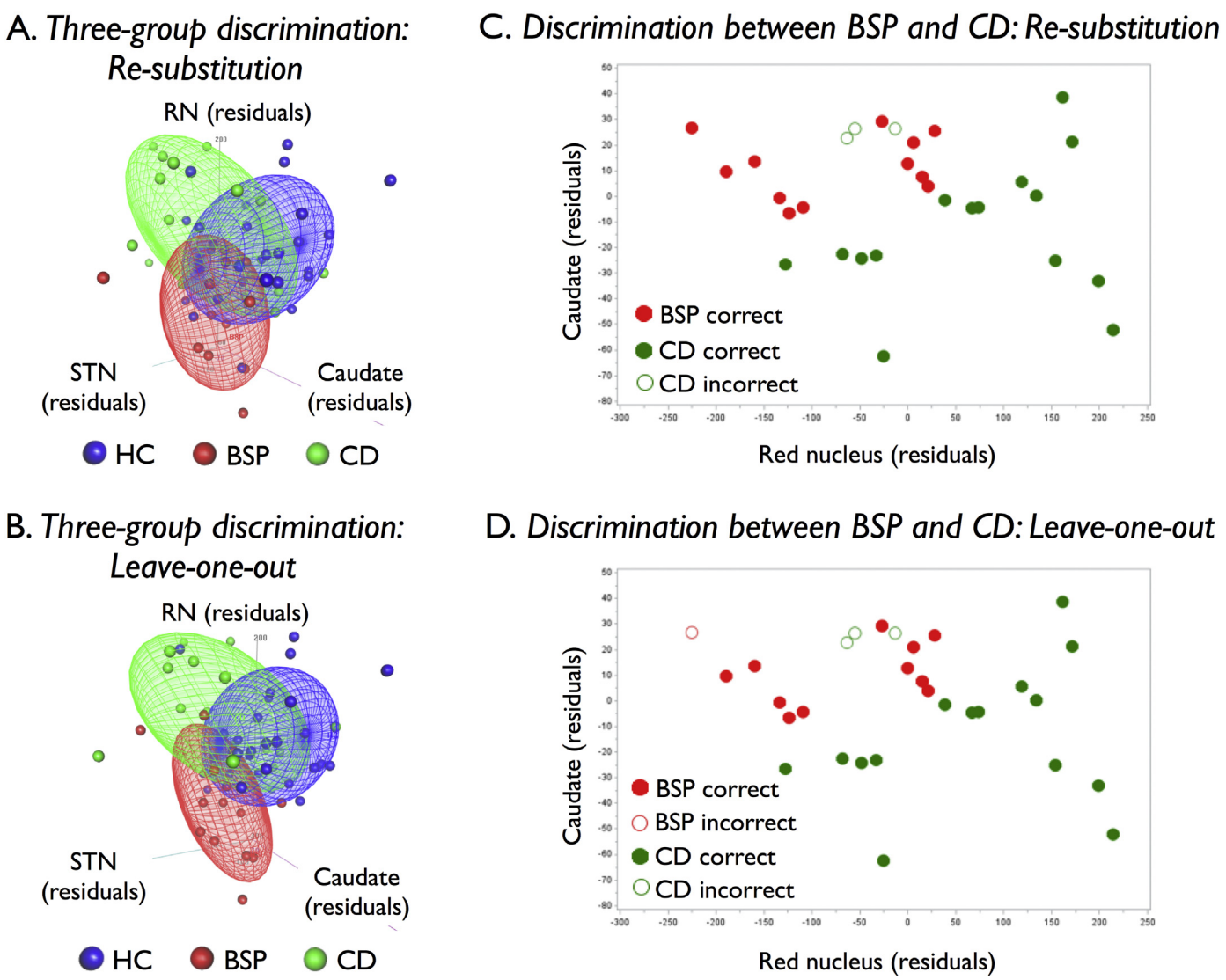

Fig. 2. Post hoc three-group A) re-substitution and B) leave-one-out discriminant analyses using mean residual fractional anisotropy (FA) values within the left red nucleus (RN), right subthalamic nucleus (STN), and left caudate following removal of the effects of age, sex, and MR scanner through regression. Correctly classified healthy controls (HC), blepharospasm (BSP) patients, and cervical dystonia (CD) patients are contained with their colored distribution clouds while misclassified participants lie outside their respective distribution clouds. Post hoc two-dimensional C) re-substitution and D) leave-one-out discriminant analyses using mean residual FA values within the left RN and left caudate correctly classified all of the BSP patients and 15 of the 18 CD patients.

globus pallidus of BSP patients is supported by a recent DTI study by Yang et al. where increased diffusivity in the right lentiform nucleus and thalamus of a separate cohort of patients with BSP (Yang et al., 2014). In their study, Yang et al. also reported that FA was reduced in the left anterior lobe of the cerebellum and that FA reductions within the white matter of the left cerebellum negatively correlated with disease severity as measured by the JRS in BSP patients. This finding along with our own finding of a link between microstructural changes within the red nucleus and JRS scores further supports a role for cerebellar afferents contributing to symptom severity in BSP. Intriguingly, the left-sided cerebellar findings in both studies suggests that there may be asymmetric pathophysiological mechanisms underlying BSP.

While our results may at first appear to differ from those reported by Pinheiro et al. who found no significant differences in white matter microstructure between groups including BSP patients, CD patients and HC (Pinheiro et al., 2015), their study differed from ours in a few key ways that likely account for the dissimilar findings. First, their dystonia population was more heterogenous division into subgroups resulted in their pure BSP subgroup including only five subjects. Second, their analysis was focused on looking for changes in *white matter* microstructure using tract-based spatial statistics, which assesses FA along major white matter tracts, while our voxel-wise approach was not restricted to white matter. And third, their ROI analysis was based on obtaining an average FA for all white matter voxels and not a ROI-based analysis using a high-resolution atlas to evaluate the microstructure of subcortical gray matter structures and brainstem nuclei.

In CD patients, both the voxel-based and ROI-based analyses revealed microstructural changes within the caudate that were not present in BSP patients. While altered FA and diffusivity involving the caudate has previously been reported in CD (Bonilha et al., 2007; Colosimo et al., 2005; Fabbrini et al., 2008), DTI changes within the caudate have not been previously reported in BSP patients (Defazio et al., 2017). Indeed, the caudate may hold particular relevance to CD as it has long been linked to head-turning in stimulation studies and found to play a role in the control of orienting reflexes (Akaike et al., 1989; Kitama et al., 1991; Murer and Pazo, 1993). In addition to the left caudate findings, we found CD patients had decreased FA in their right posterior cerebellar cortex. DTI changes affecting the cerebellum in CD were also reported by Blood et al., who found decreased FA in the left cerebellar white matter of CD patients (Blood et al., 2012). Overall, our

findings add further support to a growing body of literature that abnormal structural-functional relationships affecting striato-thalamo-cortical cerebello-thalamo-cortical networks underlies both hereditary and sporadic forms of dystonia (Carbon and Eidelberg, 2009; Kaji et al., 2018; Niethammer et al., 2011; Simonyan and Ludlow, 2012).

DTI enables the characterization of the diffusion of water molecules and can provide measures of microscopic tissue properties including density, diameter, axonal and dendritic architecture, and degree of myelination (Tournier et al., 2011). The cause of the diffusion changes we detected within the basal ganglia, brainstem and cerebellum in patients with BSP and CD, however, is not known. One possible explanation is that cell morphology has been altered within brain gray matter structures because of neuronal overactivity (due to a loss of inhibition) and/or abnormal neuroplasticity—key pathophysiological processes that have been linked to isolated dystonia (Hallett, 2011; Quartarone and Pisani, 2011). The presence of subtle structural abnormalities involving the basal ganglia and cerebellum in isolated focal dystonia is supported by a large number of MRI-based volumetric studies (reviewed in Jinnah et al., 2017), though there has not been a consistent pattern of anatomical changes across these studies. Another possible explanation for the microstructural changes seen in the focal dystonia subtypes could be the accumulation of iron, which and is known to have an effect on DTI measures of anisotropy and diffusivity, especially in deep gray matter structures (Pujol et al., 1992; Thomas et al., 1993; Xu et al., 2015). Iron plays an important role in several neuronal functions including synaptic plasticity, and the control of iron entry is tightly linked to synaptic activity (Codazzi et al., 2015). Thus, in BSP and CD iron homeostasis may be regionally altered by the pathophysiological processes of abnormal plasticity and overactivity of neurons due to loss of normal inhibitory mechanisms. Regardless of the cause of the microstructural changes we detected, a limitation of our study that is shared by other similar neuroimaging investigations in dystonia is that it is not possible to establish at this time whether these changes reflect a cause or consequence of the dystonic movements.

To date, only a few DTI studies in dystonia to date have investigated whether changes differ between CD and BSP phenotypes (Fabbrini et al., 2008; Pinheiro et al., 2015; Yang et al., 2014). None of these prior studies, however, applied probabilistic atlas maps derived using the superior anatomical resolution of a 7 T MRI to investigate gray matter structures including smaller nuclei within the basal ganglia and brainstem. To evaluate whether DTI could aid in the diagnosis of BSP and CD, we conducted post hoc discriminant analyses using FA measures within the gray matter structures that showed significant group differences. As BSP patients were characterized by lower residual FA values for the left red nucleus and higher values for the right subthalamic nucleus, and CD patients were characterized by lower residual FA values for the left caudate, we used these three structures to test the ability of DTI to differentiate between dystonia patients and HC. While the BSP and CD data distributions mostly separated, the HC distribution was largely sandwiched between them and overlapped with the two patient group distributions. This led to a modest ability to discriminate across groups from 67 to 75% using a re-substitution method, and an even poorer discriminant ability of 56 to 67% using leave-one-out cross validation. By applying a two-dimensional discriminant post hoc analysis, however, we showed that the FA measures within the left red nucleus and left caudate could distinguish BSP and CD patients with high reliability. While distinguishing these phenotypes of focal dystonia is not considered a clinical challenge, these findings support distinct pathophysiological pathways underlie these two forms of focal dystonia.

A strength of this study is that patients included in the imaging analysis were all carefully examined and only those without evidence of dystonia involvement beyond their primary site were included so that only pure phenotypic forms of focal dystonia were included. Enrollment of mixed phenotypes or lack of precise patient selection may have contributed to some of the lack of consistent DTI findings reported thus far in BSP and CD (Blood et al., 2012; Neychev et al., 2011; Pinheiro et al., 2015; Ramdhani and Simonyan, 2013; Yang et al., 2014; Zoons et al., 2011). One potential limitation to our study is the change of MRI scanners that occurred during conduction of this study. Although this could add some variance to the DTI measures used in this study, the scanner change occurred approximately midway through study enrollment, we included scanner type as a variable in our analyses, and the significance of our results is potentially strengthened as detection of true microstructural abnormalities should not be dependent on a specific scanner used. Another potential limitation in our study is that the subcortical and brainstem ROIs are small and therefore derived DTI measures may be subject to wide variance if not accurately placed. To limit this source of error, all ROIs were registered to each individual's FA map and then their placement was verified visually by a neuroradiologist (J.M.H) who was blinded to the participant's disease state.

5. Conclusions

In sum, our results support the presence of distinct microstructural changes affecting basal ganglia and cerebellar circuit nodes in BSP and CD. In particular, FA was reduced in the red nucleus and globus pallidus internus of BSP patients, and FA was reduced in the cerebellar cortex and caudate of CD patients. FA changes within the red nucleus in BSP patients were significantly correlated with disease severity, and the FA changes in the red nucleus and caudate were specific enough to their dystonia phenotype that they could reliably discriminate BSP from CD. These findings advance our understanding of the underlying pathophysiology of isolated focal dystonia phenotypes and support that microstructural changes within distinct nodes of the basal ganglia and cerebellar motor circuits could underlie the manifestation of different focal dystonia phenotypes.

Acknowledgments

We thank Debra Singel for her assistance with scanning all of our study participants and are grateful to all the volunteers for participating in the study.

Funding

This work was supported by the Dana Foundation (David Mahoney Neuroimaging Grant Program), NIH/NCATS Colorado CTSI Grant Number KL2TR002534, Benign Essential Blepharospasm Research Foundation (Research Grant), and the University of Colorado Center for NeuroScience (Innovation Award).

Financial disclosure/conflict of interest

Nothing to report concerning the research related to the manuscript.

References

Akaike, N., Ohno, T., Tsubokawa, H., 1989. EMG activities of neck muscles underlying lateral flexion of the neck during head-turning induced by electrical stimulation of the caudate nucleus in cats. Neurosci. Res. 6, 397–410.

Blood, A.J., Kuster, J.K., Woodman, S.C., Kirlic, N., Makhlouf, M.L., Multhaupt-Buell, T.J., Makris, N., Parent, M., Sudarsky, L.R., Sjalander, G., Breiter, H., Breiter, H.C., Sharma, N., 2012. Evidence for altered basal ganglia-brainstem connections in cervical dystonia. PLoS One 7, e31654.

Bologna, M., Berardelli, A., 2017. Cerebellum: an explanation for dystonia? Cerebellum Ataxias 4, 6.

Bonilha, L., de Vries, P.M., Vincent, D.J., Rorden, C., Morgan, P.S., Hurd, M.W., Besenski, N., Bergmann, K.J., Hinson, V.K., 2007. Structural white matter abnormalities in patients with idiopathic dystonia. Mov. Disord. 22, 1110–1116.

Carbon, M., Eidelberg, D., 2009. Abnormal structure-function relationships in hereditary dystonia. Neuroscience 164, 220–229.

Chapman, P.F., Steinmetz, J.E., Thompson, R.F., 1988. Classical conditioning does not occur when direct stimulation of the red nucleus or cerebellar nuclei is the unconditioned stimulus. Brain Res. 442, 97–104.

Codazzi, F., Pelizzoni, I., Zacchetti, D., Grohovaz, F., 2015. Iron entry in neurons and

astrocytes: a link with synaptic activity. Front. Mol. Neurosci. 8, 18.
Colosimo, C., Pantano, P., Calistri, V., Totaro, P., Fabbrini, G., Berardelli, A., 2005. Diffusion tensor imaging in primary cervical dystonia. J. Neurol. Neurosurg. Psychiatry 76, 1591–1593.
Consky, E., Lang, A., 1994. Clinical Assessments of Patients with Cervical Dystonia. Marcel Dekker, Inc., New York, NY.
Damian, A.M., Jacobson, S.A., Hentz, J.G., Belden, C.M., Shill, H.A., Sabbagh, M.N., Caviness, J.N., Adler, C.H., 2011. The Montreal cognitive assessment and the mini-mental state examination as screening instruments for cognitive impairment: item analyses and threshold scores. Dement. Geriatr. Cogn. Disord. 31, 126–131.
Defazio, G., Hallett, M., Jinnah, H.A., Conte, A., Berardelli, A., 2017. Blepharospasm 40 years later. Mov. Disord. 32, 498–509.
Fabbrini, G., Pantano, P., Totaro, P., Calistri, V., Colosimo, C., Carmellini, M., Defazio, G., Berardelli, A., 2008. Diffusion tensor imaging in patients with primary cervical dystonia and in patients with blepharospasm. Eur. J. Neurol. 15, 185–189.
Hallett, M., 2011. Neurophysiology of dystonia: the role of inhibition. Neurobiol. Dis. 42, 177–184.
Jankovic, J., Kenney, C., Grafe, S., Goertelmeyer, R., Comes, G., 2009. Relationship between various clinical outcome assessments in patients with blepharospasm. Mov. Disord. 24, 407–413.
Jinnah, H.A., Berardelli, A., Comella, C., Defazio, G., Delong, M.R., Factor, S., Galpern, W.R., Hallett, M., Ludlow, C.L., Perlmutter, J.S., Rosen, A.R., Dystonia Coalition, I., 2013. The focal dystonias: current views and challenges for future research. Mov. Disord. 28, 926–943.
Jinnah, H.A., Neychev, V., Hess, E.J., 2017. The anatomical basis for dystonia: the motor network model. Tremor. Other Hyperkinet. Mov. (N Y) 7, 506.
Kaji, R., Bhatia, K., Graybiel, A.M., 2018. Pathogenesis of dystonia: is it of cerebellar or basal ganglia origin? J. Neurol. Neurosurg. Psychiatry 89 (5), 488–492.
Keuken, M.C., Bazin, P.L., Crown, L., Hootsmans, J., Laufer, A., Muller-Axt, C., Sier, R., van der Putten, E.J., Schafer, A., Turner, R., Forstmann, B.U., 2014. Quantifying inter-individual anatomical variability in the subcortex using 7 T structural MRI. NeuroImage 94, 40–46.
Kitama, T., Ohno, T., Tanaka, M., Tsubokawa, H., Yoshida, K., 1991. Stimulation of the caudate nucleus induces contraversive saccadic eye movements as well as head turning in the cat. Neurosci. Res. 12, 287–292.
Klemm, W.R., Bratton, G.R., Hudson, L.C., Sherry, C.J., Dziezyc, J., 1993. A possible feline model for human blepharospasm. Neurol. Res. 15, 41–45.
Lehéricy, S., Tijssen, M., Vidailhet, M., Kaji, R., Meunier, S., 2013. The anatomical basis of dystonia: current view using neuroimaging. Mov. Disord. 28, 944–957.
Lohmann, K., Klein, C., 2017. Update on the genetics of dystonia. Curr. Neurol. Neurosci. Rep. 17, 26.
Morcuende, S., Delgado-Garcia, J.M., Ugolini, G., 2002. Neuronal premotor networks involved in eyelid responses: retrograde transneuronal tracing with rabies virus from the orbicularis oculi muscle in the rat. J. Neurosci. 22, 8808–8818.
Murer, M.G., Pazo, J.H., 1993. Behavioral responses induced by electrical stimulation of the caudate nucleus in freely moving cats. Behav. Brain Res. 57, 9–19.
Neychev, V.K., Gross, R.E., Lehericy, S., Hess, E.J., Jinnah, H.A., 2011. The functional neuroanatomy of dystonia. Neurobiol. Dis. 42, 185–201.
Niethammer, M., Carbon, M., Argyelan, M., Eidelberg, D., 2011. Hereditary dystonia as a neurodevelopmental circuit disorder: evidence from neuroimaging. Neurobiol. Dis. 42, 202–209.
Nowak, A.J., Marshall-Goodell, B., Kehoe, E.J., Gormezano, I., 1997. Elicitation, modification, and conditioning of the rabbit nictitating membrane response by electrical stimulation in the spinal trigeminal nucleus, inferior olive, interpositus nucleus, and red nucleus. Behav. Neurosci. 111, 1041–1055.
Pinheiro, G.L., Guimaraes, R.P., Piovesana, L.G., Campos, B.M., Campos, L.S., Azevedo, P.C., Torres, F.R., Amato-Filho, A.C., Franca Jr., M.C., Lopes-Cendes, I., Cendes, F., D'Abreu, A., 2015. White matter microstructure in idiopathic craniocervical dystonia. Tremor. Other Hyperkinet. Mov. (N Y) 5.
Pong, M., Horn, K.M., Gibson, A.R., 2008. Pathways for control of face and neck musculature by the basal ganglia and cerebellum. Brain Res. Rev. 58, 249–264.
Prudente, C., Hess, E., Jinnah, H., 2014. Dystonia as a network disorder: what is the role of the cerebellum? Neuroscience 260, 23–35.
Pujol, J., Junque, C., Vendrell, P., Grau, J.M., Marti-Vilalta, J.L., Olive, C., Gili, J., 1992. Biological significance of iron-related magnetic resonance imaging changes in the brain. Arch. Neurol. 49, 711–717.
Quartarone, A., Pisani, A., 2011. Abnormal plasticity in dystonia: disruption of synaptic homeostasis. Neurobiol. Dis. 42, 162–170.
Ramdhani, R.A., Simonyan, K., 2013. Primary dystonia: conceptualizing the disorder through a structural brain imaging lens. Tremor. Other Hyperkinet. Mov. (N Y) 3.
Schwarz, S.T., Abaei, M., Gontu, V., Morgan, P.S., Bajaj, N., Auer, D.P., 2013. Diffusion tensor imaging of nigral degeneration in Parkinson's disease: a region-of-interest and voxel-based study at 3 T and systematic review with meta-analysis. Neuroimage Clin. 3, 481–488.
Shakkottai, V.G., Batla, A., Bhatia, K., Dauer, W.T., Dresel, C., Niethammer, M., Eidelberg, D., Raike, R.S., Smith, Y., Jinnah, H.A., Hess, E.J., Meunier, S., Hallett, M., Fremont, R., Khodakhah, K., Ledoux, M.S., Popa, T., Gallea, C., Lehericy, S., Bostan, A.C., Strick, P.L., 2017. Current opinions and areas of consensus on the role of the cerebellum in dystonia. Cerebellum 16, 577–594.
Simonyan, K., Ludlow, C.L., 2012. Abnormal structure-function relationship in spasmodic dysphonia. Cereb. Cortex 22, 417–425.
Snook, L., Plewes, C., Beaulieu, C., 2007. Voxel based versus region of interest analysis in diffusion tensor imaging of neurodevelopment. NeuroImage 34, 243–252.
Srivastava, S., Bhatia, M.S., Bhargava, S.K., Kumari, R., Chandra, S., 2016. A diffusion tensor imaging study using a voxel-based analysis, region-of-interest method to analyze white matter abnormalities in first-episode, treatment-naive major depressive disorder. J. Neuropsychiatr. Clin. Neurosci. 28, 131–137.
Standaert, D., 2011. Update on the pathology of dystonia. Neurobiol. Dis. 42, 148–151.
Thomas, L.O., Boyko, O.B., Anthony, D.C., Burger, P.C., 1993. MR detection of brain iron. AJNR Am. J. Neuroradiol. 14, 1043–1048.
Tournier, J., Mori, S., Leemans, A., 2011. Diffusion tensor imaging and beyond. Magn. Reson. Med. 65, 1532–1556.
Vaillancourt, D.E., Spraker, M.B., Prodoehl, J., Abraham, I., Corcos, D.M., Zhou, X.J., Comella, C.L., Little, D.M., 2009. High-resolution diffusion tensor imaging in the substantia nigra of de novo Parkinson disease. Neurology 72, 1378–1384.
Wang, F., Kalmar, J.H., Edmiston, E., Chepenik, L.G., Bhagwagar, Z., Spencer, L., Pittman, B., Jackowski, M., Papademetris, X., Constable, R.T., Blumberg, H.P., 2008. Abnormal corpus callosum integrity in bipolar disorder: a diffusion tensor imaging study. Biol. Psychiatry 64, 730–733.
Xu, X., Wang, Q., Zhong, J., Zhang, M., 2015. Iron deposition influences the measurement of water diffusion tensor in the human brain: a combined analysis of diffusion and iron-induced phase changes. Neuroradiology 57, 1169–1178.
Yang, J., Luo, C., Song, W., Guo, X., Zhao, B., Chen, X., Huang, X., Gong, Q., Shang, H.F., 2014. Diffusion tensor imaging in blepharospasm and blepharospasm-oromandibular dystonia. J. Neurol. 261, 1413–1424.
Zollanvaria, A., Braga-Neto, U., Dougherty, E., 2009. On the sampling distribution of resubstitution and leave-one-out error estimators for linear classifiers. Pattern Recogn. 42, 2705–2723.
Zoons, E., Booij, J., Nederveen, A., Dijk, J., Tijssen, M., 2011. Structural, functional and molecular imaging of the brain in primary focal dystonia—a review. NeuroImage 56, 1011–1020.